Andreea Pavel

Verification of a full-order observer design for sensorless induction motor drives

School of Electrical Engineering

Thesis submitted for examination for the degree of Master of Science in Technology.

Espoo 03.03.2014

Thesis supervisor and advisor:

Prof. Marko Hinkkanen

Aalto University
School of Electrical
Engineering

AALTO UNIVERSITY
SCHOOL OF ELECTRICAL ENGINEERING

ABSTRACT OF THE
MASTER'S THESIS

Author: Andreea Pavel

Title: Verification of a full-order observer design for sensorless induction motor drives

Date: 03.03.2014 Language: English Number of pages: 6+32

Department of Electrical Engineering

Professorship: Electric Drives Code: S-81

Supervisor and instructor: Prof. Marko Hinkkanen

The main topic of this thesis is the full-order flux observer as a part of the induction machine sensorless drives. First the induction machine inverse-Γ model is presented with a brief overview of space vectors and different coordinate systems. Sensorless vector control principles and theory are presented next. Two very promising full-order observer designs were chosen, presented and tested through computer simulations. The simulations were implemented with the MATLAB/Simulink environment. The full-order observer designs are tried in different situations, like speed reversal, basic load tasks while running at a given speed, or a speed higher than the nominal to see how the design behaves. There is also a trial for stator resistance error, which can signify changes in the resistance due to temperature fluctuations or estimation errors from the mathematical model. From the test results it has been concluded that the original design is hard to tune, and it does not have tolerance to stator resistance changes. The improved design has brought more flexibility in terms of tuning, and there is a better tolerance for stator resistance changes.

Keywords: flux estimation, full-order observer design, induction motor drives, sensorless vector control

Acknowledgement

I firstly want to give my gratitude to my supervisor and advisor Marko Hinkkanen for his help, and advices with writing my first time in English. He was always available to answer my doubts and guide me through my struggles with this thesis. I will always feel grateful also for allowing me to write the thesis in the Electrical Engineering Department of Aalto University.

I wish to thank my friends here in Finland for their continuous support when I was feeling discouraged. Lastly I want to thank my parents for helping me come here, in Finland, for their support, and for always pushing me forward.

Thank you.

Otaniemi, March 3, 2014

Andreea Pavel

Contents

Symbols and abbreviations

Symbols

$*$	represents a complex conjugate
$\hat{}$	represents the estimates of the variables
$\dot{}$	represents the derivative
$_s$	represents the variables in the stator coordinates
$_{d,q}$	components of a vector in synchronous coordinates
$_B$	base values of the motor
$_N$	nominal values of the motor
$_{ref}$	represents the reference of the variable
$_{\alpha,\beta}$	components of a vector in stator coordinates
$\mathbf{A}, \mathbf{B}, \mathbf{C}$	state matrices
$d_{a,b,c}$	duty cycles
f_1	nominal frequency
$\mathbf{G}$	observer gain matrix
$\mathbf{i}_s$	stator current
$\mathbf{i}_R$	rotor current
$\mathbf{i}_M$	magnetizing current
Im	imaginary part of a complex number
j	imaginary unit
J	total mechanical inertia
L_σ	total leakage inductance
L_M	magnetizing inductance
Re	real part of a complex number
r, l, x	observed design free parameters
R_s	stator resistance
R_R	rotor resistance
p	number of pole pairs
$p.u.$	per unit
s	Laplace operator
t	time
T_e	electromagnetic torque
T_L	load torque
T_r	rotor time constant
$\mathbf{u}$	voltage vector in synchronous coordinates
u_a, u_b, u_c	phase voltages
u_{dc}	dc-link voltage
$\mathbf{x} = [\mathbf{i}_s \ \boldsymbol{\psi}_R]^T$	state vector
$z, \omega_\delta, \omega_{min}$	gain selection design parameters
ϵ	error of the speed adaptation
$\gamma_{p,i}$	speed adaptation gains
ω_1	synchronous speed, stator angular speed
ω_r	electrical rotor speed
$\boldsymbol{\psi}_s$	stator flux linkage
$\boldsymbol{\psi}_R$	rotor flux linkage
ψ_R	magnitude of $\boldsymbol{\psi}_R$
σ	total leakage factor
θ_1	rotor flux angle

Abbreviations

AC	alternative current
DFO	direct field orientation
IFO	indirect field orientation
IM	induction machine
ISFE	inherently sensorless flux estimator
MRAS	model reference adaptive system
PWM	pulse width modulation
RFO	rotor flux orientation
ROO	reduced-order observer
FOO	full-order observer
v/f	voltage-to-frequency
VM	voltage model

1 Introduction

The induction machine (IM), also known under the name of asynchronous machine, was invented separately by two scientist: Galileo Ferraris in 1885 and Nicola Tesla in 1887. The two induction machines were different in construction but they were working on the same principle. From this point, a lot of improvement has been done to the construction of the machine, bringing the machine to have a higher efficiency and better performance, but the principle has not been changed from the initial invention.

The IM is chosen in applications because of its many advantages, which are: low price, high durability, simple design, ease of manufacture, and small losses. The biggest drawback for the IM was the challenging control of the speed. Due to great improvements in power electronics and electric drives, the usage of induction machine in applications with variable speed has increased considerably, making the induction machine as the main means to produce mechanical energy in the world. The motor is used in a wide range of applications from industry to home appliances. The IM has as main advantage the possibility to connect directly to the grid, but there is no control of the motor's speed this way.

There are several methods which are used to control an induction motor. The most popular method is voltage-to-frequency (v/f) control, which is a simple scalar control method. This method consists of an open loop that does not require feedback from the machine, but the speed cannot be controlled precisely. Scalar control is a simple method of control. The main disadvantage of the scalar control is that in transients there are large and fast increases in the stator current which is undesirable. It also presents a slow response for speed or torque reference changes. For more intricate applications that require better performance in terms of torque and speed control, scalar control is not enough. In order for the speed control to be more accurate, vector control was developed. Vector control is more complicated because it involves a model of the machine, current and speed controllers, several coordinates transformations and, depending if there are no measurements for speed, full-order or reduced-order observers are introduced in the control scheme.

The speed-sensorless drive has a lot of advantages, the most significant being the reduction in price, but the decrease in size and maintenance of the drive is also attractive for potential customers. These advantages are brought by eliminating cables, sensors, and noise from the whole system, otherwise the system would be a lot bigger. Hence, the drive is suitable for applications that require the machine to be put in tight spaces.

There are some disadvantages for sensorless control, which are very crucial to the safety performance of the drive. One of these disadvantages is operating in the low speed region, especially if a considerable load is connected to the shaft of the machine. This is caused mainly by the inaccurate estimation of speed and flux, which are calculated by a digital signal processor, using as inputs the voltages and stator currents. It is still challenging to be able to design a sensorless flux observer that has good performance at low speeds and for the regenerative mode operating at normal load torque. The full-order observer designs will "always be marginally

stable for zero stator frequency."[1].

In this thesis the focus is on speed-sensorless induction motor drives. To achieve the speed-sensorless operation, the flux and also the speed need to be estimated. In this thesis a speed-adaptive full-order observer proposed in [2] was chosen as preference to estimate the two variables. The speed-adaptive full-order observer is a state-variable observer to which a speed-adaptation loop is added. The papers [3] and [4] are recent promising designs for such a full-order observer. The main task for this thesis is to evaluate them by means of computer simulations in order to determine their stability and how easy it is to implement them to a control scheme already designed.

The thesis is structured in six chapters: Chapter 2 contains basic knowledge needed to understand vector control, which are space vector theory, coordinates transformations, and the inverse-Γ model. Chapter 3 presents general information about sensorless vector control. In Chapter 4 a full-order observer is described and also the designs proposed in [3] and [4] are presented. Chapter 5 consists of the computer simulations conducted and the results and Chapter 6 shows discussions and conclusions.

2 Induction machine model

2.1 Space vectors and synchronous coordinates

To model the induction machine, a little introduction in space vectors is needed to understand the equations and variables used for modelling the machine. Ideally the induction machine is supplied by a symmetric three-phase system.

With the help of space vectors, the three-phase system can be written as a two-phase system, thus making the system easier to model and control. The two-phase system can be represented in a complex plane, which has two perpendicular axes, α being the real axis and β being the imaginary axis.

Space vectors

A space vector $\mathbf{u}^s(t)$ consists of two components, one real and one imaginary:

$$\mathbf{u}^s(t) = u_\alpha(t) + ju_\beta(t) \tag{2.1}$$

where the superscript "s" means that the system is in stator coordinates which is stationary and j is the imaginary unit. The space vector is formed from the three-phase system with

$$\mathbf{u}^s(t) = \frac{2}{3}\left(u_a(t) + e^{j\frac{2\pi}{3}}u_b(t) + e^{j\frac{4\pi}{3}}u_c(t)\right) \tag{2.2}$$

where $u_a(t), u_b(t), u_c(t)$ are the three-phase stator voltages.

If the machine is delta connected or there is no neutral connection for a wye connection the zero-sequence component of the three-phase supply is not transmitted to the three-phase currents. Therefore, the zero-sequence component can be neglected.

To achieve a reverse transformation from the three-phase system to the two-phase system, these equations are used:

$$\begin{cases} u_a(t) = \mathrm{Re}\left\{\mathbf{u}^s(t)\right\} \\ u_b(t) = \mathrm{Re}\left\{\mathbf{u}^s(t)e^{j\frac{4\pi}{3}}\right\} \\ u_c(t) = \mathrm{Re}\left\{\mathbf{u}^s(t)e^{j\frac{2\pi}{3}}\right\} \end{cases} \tag{2.3}$$

Synchronous coordinates

A space vector transformed from the $\alpha\beta$ *coordinates* into synchronous coordinates means that the system of reference is changed from a stationary one to a rotating system that typically revolves in time with some space vector. This transformation is realized by

$$\mathbf{u} = e^{-j\theta_1}\mathbf{u}^s \tag{2.4}$$

where $\theta_1 = \int \omega_1 dt$ is the angle of the rotating coordinate system, ω_1 is the angular speed of the rotating coordinate system, and $\mathbf{u} = u_d + ju_q$.

The reverse transformation from synchronous coordinates to $\alpha\beta$ *coordinates* is

$$\mathbf{u}^s = e^{j\theta_1}\mathbf{u} \tag{2.5}$$

The transformation for a time derivative to synchronous coordinates:

$$s \rightarrow (s + j\omega_1) \tag{2.6}$$

where s is the Laplace operator which replaces the derivative.

2.2 Construction and operation of the induction machine

The induction machine has a fixed part, the stator, and a mobile part, the rotor. The stator is a hollow cylinder composed of thin laminated electromagnetic steel sheets, which on the inner surface have slots cut into them, in which a three phase winding will be put. The rotor of the induction machine is also a cylinder made of thin laminations, which can be a squirrel-cage type or a wound-rotor type. The most common one is the squirrel-cage type because of ease of manufacturing and economical reasons. The squirrel cage mainly means that the rotor winding, which is made of aluminium or copper bars, is short-circuited at both ends by aluminium or copper rings. The rings sometimes have a secondary role as a radiator depending on the construction. The rotor is usually skewed because it helps to smoothen the torque.

An induction machine is magnetized from the stator, unlike the synchronous machine which is magnetized from the rotor. When the stator winding is connected to the voltage supply a current flows through and produces an electromagnetic flux in the air gap which induces a current inside the short-circuited winding in the rotor, which creates an electromagnetic force that moves the rotor.

After the machine is connected to the supply, the stator flux vector rotates with the speed ω_1, also known as stator angular frequency:

$$\omega_1 = 2\pi f_1 \tag{2.7}$$

where f_1 is the frequency of the supply. This should not be mistaken with the rotor speed ω_r. Since there is a difference between the rotor speed and the stator speed, the notion of slip frequency has been introduced which is the subtraction of the rotor speed from the angular supply frequency, $\omega_1 - \omega_r$.

2.3 Inverse-Γ model

The model for the induction machine chosen to use further in this thesis is the inverse-Γ model [5], which gives more simplicity and ease of usage in vector control, unlike the T model. In this model, the rotor parameters are reconfigured, such that the two leakage inductances are represented only by one.

The stator and rotor flux linkages for the inverse-Γ model are expressed mathematically with the following expressions:

$$\begin{cases} \boldsymbol{\psi}_s^s = L_\sigma \mathbf{i}_s^s + L_M \mathbf{i}_M^s \\ \boldsymbol{\psi}_R^s = L_M \mathbf{i}_M^s \end{cases} \tag{2.8}$$

where $\boldsymbol{\psi}_s^s$ is the stator flux linkage, $\boldsymbol{\psi}_R^s$ is the rotor flux linkage, L_σ is the total leakage inductance, L_M is the magnetizing inductance, $\mathbf{i}_s^s$ is the stator current, and $\mathbf{i}_M^s$ is the magnetizing current, which is defined by

$$\mathbf{i}_M^s = \mathbf{i}_s^s + \mathbf{i}_R^s \tag{2.9}$$

where $\mathbf{i}_R^s$ is the rotor current.

Following the law of induction, it is known that the voltage is not all dissipated in the stator winding and so the remaining voltage induces a flux in the stator winding. The principle can be written in mathematical form:

$$\mathbf{u}_s^s = R_s \mathbf{i}_s^s + \frac{d\boldsymbol{\psi}_s^s}{dt} \tag{2.10}$$

where $\mathbf{u}_s^s$ is the stator voltage and R_s is the stator resistance. This principle can be applied to the rotor as well. Hence the rotor equation is as follows:

$$j\omega_r \boldsymbol{\psi}_R^s - R_R \mathbf{i}_R^s - \frac{d\boldsymbol{\psi}_R^s}{dt} = 0 \tag{2.11}$$

where R_R is the rotor resistance and ω_r is the rotor electrical speed.

The stator flux linkage in the stator voltage equation (2.10) is replaced with (2.8) and thus the system of equations for the machine becomes

$$\begin{cases} \mathbf{u}_s^s - R_s \mathbf{i}_s^s - L_\sigma \dfrac{d\mathbf{i}_s^s}{dt} - L_M \dfrac{d\mathbf{i}_M^s}{dt} = 0 \\ j\omega_r \boldsymbol{\psi}_R^s - R_R \mathbf{i}_R^s - \dfrac{d\boldsymbol{\psi}_R^s}{dt} = 0 \end{cases} \tag{2.12}$$

Due to the fact that the rotor current cannot be measured, the equations should not contain the rotor current. The rotor current will be eliminated by using (2.9) and $\mathbf{i}_M^s = \boldsymbol{\psi}_R^s / L_M$ from (2.8):

$$\begin{cases} L_\sigma \dfrac{d\mathbf{i}_s^s}{dt} = \mathbf{u}_s^s - R_s \mathbf{i}_s^s - \dfrac{d\boldsymbol{\psi}_R^s}{dt} \\ \dfrac{d\boldsymbol{\psi}_R^s}{dt} = R_R \mathbf{i}_s^s - (R_R/L_M - j\omega_r)\, \boldsymbol{\psi}_R^s \end{cases} \tag{2.13}$$

There should not be derivatives on the right side, so the derivative of the rotor flux is replaced with the second equation:

$$\begin{cases} \dfrac{d\mathbf{i}_s^s}{dt} = -\dfrac{R_s + R_R}{L_\sigma} \mathbf{i}_s^s + \dfrac{R_R/L_M - j\omega_r}{L_\sigma} \boldsymbol{\psi}_R^s + \dfrac{1}{L_\sigma} \mathbf{u}_s^s \\ \dfrac{d\boldsymbol{\psi}_R^s}{dt} = R_R \mathbf{i}_s^s - (R_R/L_M - j\omega_r)\, \boldsymbol{\psi}_R^s \end{cases} \tag{2.14}$$

The system expressed in synchronous coordinates is:

$$\begin{cases} \dfrac{d\mathbf{i}_s}{dt} = -\left(\dfrac{R_s + R_R}{L_\sigma} + j\omega_1\right)\mathbf{i}_s + \dfrac{R_R/L_M - j\omega_r}{L_\sigma}\boldsymbol{\psi}_R + \dfrac{1}{L_\sigma}\mathbf{u}_s \\ \dfrac{d\boldsymbol{\psi}_R}{dt} = R_R\mathbf{i}_s - \left[R_R/L_M + j\left(\omega_1 - \omega_r\right)\right]\boldsymbol{\psi}_R \end{cases} \tag{2.15}$$

The equation of motion is

$$\frac{d\omega_r}{dt} = \frac{p}{J}\left(T_e - T_L\right) \tag{2.16}$$

where p is the number of pole pairs, J is the total mechanical inertia of the drive system, and T_L is the mechanical load. The electromagnetic torque is expressed by the equation

$$T_e = \frac{3}{2}p\mathrm{Im}\left\{\mathbf{i}_s^s\boldsymbol{\psi}_R^{s*}\right\} \tag{2.17}$$

where $\boldsymbol{\psi}_R^{s*}$ is the complex conjugate of $\boldsymbol{\psi}_R^s$.

3 Speed-sensorless vector control

3.1 Vector control in general

Vector control is also known as field-oriented control, for which K. Hasse and F. Blaschke have developed the principles. The purpose of this method was to realize high quality control of the IM.

Field orientation can be done in many ways but these methods can be classified into two categories: direct and indirect field orientation. For the direct field orientation (DFO), the estimates are calculated in the stator coordinates, but in the case of the indirect field orientation (IFO) the calculations are done in the polar coordinates. The flux estimators implemented in DFO can have equivalent IFO flux estimators, but vice versa is not always possible. [1]

Speed sensorless vector control for IM is advantageous because it offers hardware simplicity, reduction in size of the whole drive due to elimination of the sensors and the cables required for it. All this will make the drive considerably cheap, it will require less maintenance and increased noise immunity. This kind of drive is suitable for hostile environments in which a speed sensor could be affected [6].

Vector control is more challenging than a simple volt to hertz control. Field orientation is realized by knowing the position angle, hence the flux should be measured. But flux measurement is difficult, costly, and puts limitations. Air-gap sensors limit the maximum temperature at which the machine can be used ($< 120°$C) [7]. The sensors need to be introduced while the machine is manufactured which will increase the machine's price significantly more than a standard IM's. The solution for eliminating flux measurement is a flux estimator block that will be added to the control scheme.

It would be ideal if the IM would be as easily controlled as the DC machine. Vector control makes it possible by making the IM behave dynamically the same as a DC machine through field orientation [8]. The field orientation can be done either with the stator flux or rotor flux. Rotor flux orientation (RFO) is used in this thesis, because the RFO makes it possible to control the torque and rotor flux independently of each other through the d and q components of the stator current, and because it offers ease in calculations and algorithm. In the next section the RFO will be explained briefly.

3.1.1 Rotor flux orientation

Rotor flux orientation is achieved by choosing the angle of the dq transformation to the angle of the rotor flux, $\theta_1 = \arg\boldsymbol{\psi}_R^s$. When the $\alpha\beta$ *coordinates* are transformed to dq *coordinates*, the imaginary part of the rotor flux becomes zero:

$$\boldsymbol{\psi}_R = \psi_R + j0 \tag{3.1}$$

This being inserted in (2.15) we get that

$$\frac{d\psi_R}{dt} = R_R i_{sd} - \frac{R_R}{L_M}\psi_R \tag{3.2}$$

and

$$\omega_1 - \omega_r = \frac{R_R i_{sq}}{\psi_R} \tag{3.3}$$

After doing the Laplace transformation and rearranging (3.2) we get that the flux is directly proportional to i_{sd}:

$$\psi_R = \frac{L_M i_{sd}}{sT_r + 1} \tag{3.4}$$

where $T_r = L_M/R_R$ is known as rotor time constant.

Also the torque can be deduced from (2.17) too:

$$T_e = \frac{3}{2} p i_{sq} \psi_R \tag{3.5}$$

The two equations, (3.5) and (3.2), show that the torque is directly proportional with the q component of the current and the flux with the d component. Thus the torque and flux can be controlled independently from each other by adjusting the q and d components of the stator current.

3.1.2 Speed-sensorless vector control

Beyond flux estimation, the focus is to make the drive speed-sensorless, thus eliminating the speed sensor as well. This is advantageous because of reasons stated earlier and because there is still room for development in this area. In the low-speed region, the sensorless control still has problems. The speed-sensorless control relies a lot on the speed estimation in terms of stability and accuracy. The speed estimation, ideally, should be as close to the real speed as possible so that the system has good performance.

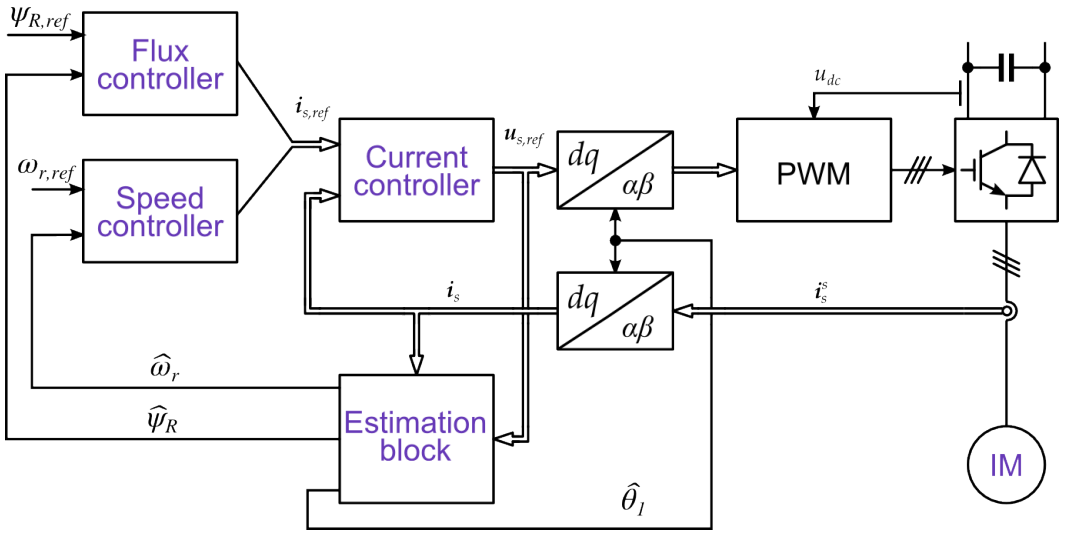

Figure 3.1: Block scheme for speed-sensorless control in the rotor reference frame [9]

Figure 3.1 represents a speed sensorless control scheme. From this scheme, the thesis concentrates on the "Estimation block". In the scheme presented, the "Estimation block" is implemented in the estimated rotor flux reference frame. However, if the "Estimation block" would get the measured current before it was transformed by the "$dq/\alpha\beta$" block, then the "Estimation block" would be in the stator reference frame. But using the stator reference frame has a setback. In this reference frame the electrical variables are oscillating sinusoidally at the stator angular speed, ω_1. This can cause the flux estimators to be unstable and/or inaccurate at high velocity [9]. The "Estimation block" is in charge of supplying the control scheme with the estimates of rotor flux, rotor speed and flux angle from the current measurement and the voltage reference, since it is assumed that the voltage reference is the same as $\mathbf{u}_s$ [9]. The estimated rotor flux and rotor speed serve as feedback to the "Flux controller" and "Speed controller", respectively. The estimated angle is used to make the necessary transformation from stator reference to synchronous coordinates and vice versa. The "Flux controller" and "Speed controller" provide with the reference for i_{sd} and i_{sq}, respectively. Finally the "Current controller" calculates the reference of the voltage needed by the "PWM" in order to send the duty cycle commands to the converter.

3.2 Flux estimators

As it was stated before, flux sensors and position sensors are impractical and are not widely used in industry, because it is easier to use a flux estimator instead. All sensors require careful handling, extra cabling, and more maintenance. The price of an IM with such sensors will be significantly higher than the price of a standard induction machine.

The flux estimator in principle is a dynamic model of the IM. The flux estimator usually uses estimated motor parameters instead of the actual parameters. It is well known that the motor parameters are fluctuating according to temperature and magnetic saturation. This determines that eventually the estimated parameters are different from the actual ones. This inaccuracy might cause torque non-linearity and magnetic saturation of the IM. The ideal flux estimator would be insensitive to fluctuating motor parameters.[10]

There are some different types of flux estimator designs proposed in [11], [2], [9]. A simple classification has been done which starts from simpler designs to more complicated ones. First there are inherently sensorless flux estimators, then there is the model reference adaptive system (MRAS), then the reduced-order observers, and finally the full-order observers which are the flux estimators needed for this thesis.

3.2.1 Inherently sensorless flux estimators (ISFEs)

The flux estimators that are named inherently sensorless are the ones that do not need the speed for estimating the flux. Since they are independent of speed estimation, the flux estimators are not affected dynamically by the speed. They

also require little computation power and time. These can be considered a good advantages that would be useful for some applications that require a cheap and fast drive.

The most simple and common of the ISFEs is the voltage model (VM), which will be briefly presented below. In [9], this model was called "pure" because the VM has been modified in many ways so that the model's setbacks would disappear or diminish. A couple of these VM variations have been proposed in [9]. Here only the VM will be presented because the ISFEs are not the focus of this thesis.

Voltage model

The name is very suggestive for this model. The VM estimates the rotor flux by using the voltage equation from (2.13):

$$\frac{d\hat{\boldsymbol{\psi}}_R^s}{dt} = \mathbf{u}_s^s - \hat{R}_s \mathbf{i}_s^s - \hat{L}_\sigma \frac{d\mathbf{i}_s^s}{dt} \tag{3.6}$$

where $\hat{R}_s$ and $\hat{L}_\sigma$ are the estimated values of the stator resistance and total leakage inductance, respectively.

The voltage model has low parameter sensitivity at medium and high speeds. At low speeds the stator resistance has critical effect on the model [1]. The VM also gives a marginal stability to the system, because the poles are on the imaginary axis [12].

3.2.2 Speed adaptive flux estimators

MRAS flux estimators

The MRAS has three main modules which can be referred to as the reference model (which does not need the speed estimation), the adjustable model (which needs the speed estimation), and the speed-adaptation law [9]. The reference model and the adjustable model estimate the same state variable which mostly is the rotor flux, as shown in [9], [6], [13], but it can also be the rotor induced voltage [6]. Most often the two flux estimators are chosen to be the voltage model and the current model, respectively [14], [9].

The MRAS can be considered as a special case of the full-order observer if the state variables are the stator and rotor fluxes. This is demonstrated in [15] by selecting the observer gain so as to obtain the voltage model and current model. The MRAS has marginal stability because its poles are on the imaginary axis [15].

Reduced-order observer

The reduced order observers (ROO) is a simpler case of the full-order observer. The ROO is used to estimate only one of the state variables of the model. So a reduced-order observer will estimate either the rotor flux or the stator flux because the stator current is measurable, hence considered known variable [11]. Some designs do not need the speed, which means they are inherently sensorless. In case the speed

is needed it can be either measured or estimated. If the speed estimation is used then the drive would be speed-sensorless.

The difference between a reduced-order observer and a flux estimator is that it uses a correction error. The correction error is the subtraction between the stator voltage and its estimate. The estimated voltage is calculated using the estimated motor parameters and the estimated flux[12]. In paper [11], a few ROO designs are shown in the beginning of the paper. Recent new designs in ROO have been created and published in [16] and [17]. [16] has proposed a ROO that has a low sensitivity to rotor and stator resistance fluctuations, and can be implemented on a low-cost fixed-point DSP board. The implementation was realized with an algorithm based on look-up tables, because the design is quite complex. Whereas [16] proposed a very complicated design, [17] achieved a simpler design, which is easy to tune, and gives robustness and well-damping to the system.

Speed-adaptive full-order observer

Whereas a reduced-order observer tries to estimate only one state-variable of the machine model, a full-order observer (FOO) attempts to estimate every state variable of the machine not just the rotor or stator flux [11]. The attempt to estimate all of the variables is motivated because of the measurement noise. The estimated variables will be the same as the filtered measurements of those same variables. Many designs estimate the current besides the rotor flux or stator flux that the ROO estimates. These designs are also known as fourth-order observers.

Since the FOO is not speed-sensorless by itself, the FOO needs to be coupled with a speed estimation. Such schemes were proposed in literature by [2] and [18] under the name of speed-adaptive full-order observers. Since the speed-adaptive FOO is the vector control method chosen in this thesis, the speed-adaptive FOO will be presented in more detail in the next chapter.

4 Speed-adaptive full-order observer

A big advantage for the full-order observer is that it offers tolerability to measurement noise and robustness against parameter sensitivity. Thanks to these the full-order observer preforms well, although the gain selection can control the parameter sensitivity [19]. The FOO is also quite flexible, different design schemes can be analysed with the same tools and with same experimental algorithms [9].

The full-order observer has a few disadvantages, that some are diminished as new research is published. The FOO is a non-linear system due to using the speed in the state matrix. Hence the dynamics of the observer are easily affected by the speed-adaptation loop [15]. The low speed region is a well known problematic area for all sensorless schemes, especially if the motor runs in the regenerative mode as stated in [9], [15], [20].

The gains should be carefully selected because higher speed operation has a risk of becoming unstable due to badly selected gains or if the gains are chosen to be zero [15], which is the conventional way. The gains can affect the range of the speed and the stability in the field-weakening region also. The full-order observer gains can be simply chosen as zero, like it was chosen in [2], but the observer gains can be designed using the pole placement or stability analysis like it was proposed in [15] and [3].

For the full-order flux observer to work accurately and stably when the motor operates at high speeds and normal speeds, high-order discretization methods are needed which require lot of computation time and computational power. A simple method is proposed in [19].

The purpose of this thesis is to verify the reliability and stability of the new promising full-order observer designs that were proposed in [3] and [4]. These proposed designs will be presented later on in this chapter.

4.1 General representation of a full-order observer

In order to represent the FOO, a state-space system is needed. A state-space system can be represented as:

$$\begin{cases} \dot{\mathbf{x}} = \mathbf{A}\mathbf{x} + \mathbf{B}\mathbf{u} \\ \mathbf{y} = \mathbf{C}\mathbf{x} \end{cases} \tag{4.1}$$

where $\mathbf{x}$ is the state vector, $\mathbf{u}$ is the input vector, and $\mathbf{y}$ is the output vector. The $\mathbf{A}$, $\mathbf{B}$, and $\mathbf{C}$ are the system matrices.

Following the state-space system above, a state-space representation of the in-

duction machine model in synchronous coordinates can be achieved:

$$\begin{cases} \begin{bmatrix} \dot{\mathbf{i}}_s \\ \dot{\boldsymbol{\psi}}_R \end{bmatrix} = \underbrace{\begin{bmatrix} -\dfrac{R_s+R_R}{L_\sigma} - j\omega_1 & \dfrac{R_R/L_M - j\omega_r}{L_\sigma} \\ R_R & -\left[R_R/L_M - j\left(\omega_r - \omega_1\right)\right] \end{bmatrix}}_{\mathbf{A}} \underbrace{\begin{bmatrix} \mathbf{i}_s \\ \boldsymbol{\psi}_R \end{bmatrix}}_{\mathbf{x}} + \underbrace{\begin{bmatrix} \dfrac{1}{L_\sigma} \\ 0 \end{bmatrix}}_{\mathbf{B}} \mathbf{u}_s \\ \mathbf{i}_s = \underbrace{\begin{bmatrix} 1 & 0 \end{bmatrix}}_{\mathbf{C}} \begin{bmatrix} \mathbf{i}_s \\ \boldsymbol{\psi}_R \end{bmatrix} \end{cases} \tag{4.2}$$

In order to represent the IM model state-space representation, the $\mathbf{i}_s$ and $\boldsymbol{\psi}_R$ were chosen as state variables so that there is a continuation from the inverse-Γ model from chapter 2 and because they are the conventional state variables. However in papers such as [9], and [15] the stator and rotor flux are chosen as state variables instead of the stator current and rotor flux, due to some advantages. By choosing the fluxes the observer is more flexible in the sense that it can be used also with stator flux orientation control and direct torque control, beside the rotor orientation control. Also the modelling of magnetic saturation is simpler [15].

A full-order observer has the same form as a state-space representation, only that an error correction is added to the equation. A general form of a full-order observer applied for the induction machine model is

$$\dot{\hat{\mathbf{x}}} = \hat{\mathbf{A}}\hat{\mathbf{x}} + \mathbf{B}\mathbf{u}_s + \mathbf{G}(\mathbf{i}_s - \hat{\mathbf{i}}_s) \tag{4.3}$$

where

$$\hat{\mathbf{A}} = \begin{bmatrix} -\dfrac{R_s+R_R}{L_\sigma} - j\omega_1 & \dfrac{R_R/L_M - j\hat{\omega}_r}{L_\sigma} \\ R_R & -\left[R_R/L_M - j\left(\hat{\omega}_r - \omega_1\right)\right] \end{bmatrix} \quad \text{and} \quad \mathbf{G} = \begin{bmatrix} g_1 + jg_2 \\ h_1 + jh_2 \end{bmatrix} \tag{4.4}$$

In order to achieve a speed-adaptive FOO, the estimation of the speed is needed like it was proposed in [2]. In this case, the conventional speed-adaptive law is used:

$$\hat{\omega}_r = -\gamma_p \varepsilon - \gamma_i \int \varepsilon dt \tag{4.5}$$

where γ_p and γ_i are positive adaptation gains and ε is an error term. The speed-adaptive law uses the error between the measured current and the estimated one. Thus, the error term is calculated using

$$\varepsilon = \mathrm{Im}\left\{(\mathbf{i}_s^s - \hat{\mathbf{i}}_s^s)\boldsymbol{\psi}_R^{s*}\right\} \tag{4.6}$$

More variations of the speed-adaptive law were presented in [9].

4.2 Original observer design

The goal of the paper [3] was to design an adaptive observer structure that would be easily adaptable to surface and interior permanent magnet synchronous motors as well, not just IMs. They have shown similar models for the machines, and concluded that the IM model can be adopted as a general model for these AC motors.

The paper [3] proposes three design strategies in order to stabilize the observer in the regenerative low-speed area. This thesis will be considering only one of them (Design A in paper[3]).

In the paper, the gains for the matrix $\mathbf{G}$ are derived in order for the positive real property conditions to be met. While the observer is implemented in stator coordinates in the paper, here the gains will be presented in the synchronous reference frame:

$$\begin{cases} g_1 = \dfrac{R_s - r}{L_\sigma} + \dfrac{R_R}{\sigma L_M} \\ g_2 = -\dfrac{x}{L_\sigma} \\ h_1 = -L_\sigma g_1 - l\dfrac{R_R}{L_M} + R_s \\ h_2 = -L_\sigma g_2 - l\hat{\omega}_r \end{cases} \tag{4.7}$$

in which the parameters r and l need to be positive, however x does not have any condition, and $\sigma = L_\sigma/(L_\sigma + L_M)$ represents the total leakage factor.

The authors of the paper [3] have provided with a design structure for the gain matrix, $\mathbf{G}$, needed for the FOO. There are still the free parameters r, l, and x to be concerned about. However they have proposed a modality of choosing the free parameters as well:

$$\begin{cases} l = L_\sigma |\hat{\omega}_r|^2 / \sqrt{R_R^2/L_M^2 + \hat{\omega}_r^2} \\ r = L_\sigma \max\{|\hat{\omega}_r|, \omega_{min}\} \\ x = L_\sigma(\hat{\omega}_r - \omega_1) \end{cases} \tag{4.8}$$

where ω_{min} is a parameter used as a limit for the low speed area.

[3] presents also some experimental results with some figures. It is shown how the design behaves in the regenerative mode for low and high speeds. It can be seen that the system becomes unstable for low speeds, and for high speeds some poor damping is observed.

4.3 Improved observer design

[4] proposes a structure for the free parameters l, r and x, having the same design framework for the gain matrix, $\mathbf{G}$, proposed in [3]. Furthermore a resistance adaptation method has been added to the observer design and analysed. There is also a comparison between the proposed FOO and the ROO chosen from [17].

In this paper, it is stated that the free parameters should vary with the speed estimate, in order to get a good performance. These parameters are affecting the properties of the system such as robustness, damping, convergence rate, and as

others [4]. This can also be seen later on in this thesis. The parameters l, r and x that were proposed in [4] are

$$\begin{cases} l = \min\left\{\dfrac{R_s L_M}{R_R}, \dfrac{z}{|\hat{\omega}_r|}\right\} \\ r = R_R + \dfrac{R_R}{L_M} l + z \cdot \min\left\{\dfrac{|\hat{\omega}_r|}{\omega_\Delta}, 1\right\} \\ x = \hat{\omega}_r l \end{cases} \tag{4.9}$$

where $z = 0.3$ p.u. and $\omega_\Delta = 0.5$ p.u.

The above parameters are chosen in such a manner that the gain matrix proposed in the original design, [4], resembles the one that is proposed in [21] when the speed reaches higher values.

The paper also uses a stator-resistance adaptation together with the observer in order to improve the low-speed instability. The stator-resistance adaptation allows to make the unstable region narrower. With this design strategy the paper [4] gives results of a well-damped, robust and stable system that are shown through theoretical as well as experimental means. The proposed FOO design is compared with the original design [3] as well as with the ROO design [17].

5 Simulations

5.1 MATLAB/Simulink

MATLAB is a well known academic and industrial software for analysing data, writing algorithms and developing applications. MATLAB has as graphic interface Simulink, in which different types of simulations and applications can be realized with the help of the block diagrams. The basic block diagrams are provided by the MATLAB/Simulink tools for which the user only needs to provide input parameters. They can also be developed based on S-function blocks or made of equation blocks, which means the user can develop his own blocks according to his preferences. The MATLAB environment has been used in this thesis for conducting simulations of an induction machine operation.

5.2 Simulation model

In Figure 5.1 the simulation model of a vector control scheme for the induction machine is shown. The blocks that construct the scheme are the "Induction machine", "Frequency converter", and "RFO". The objective of the application is to control the induction machine, which is the first block from the right. It has as inputs the load torque and stator voltage. In a physical application, there are measurements taken from the machine which in this model are the outputs. These are the stator current and the rotor speed. The simulation model itself can be modified so that the speed is also measured in order to verify the accuracy of the full order observer design and/or to simulate other vector control methods, for example: reduced-order observers which need speed sensor feedback. The speed variable is not used to control the machine.

The "RFO" block is presented in Figure 5.2. This block is the one that gives the controls signals to the frequency converter, hence this block can be identified as a vector control module. The "RFO" contains the control blocks necessary to control the speed, flux, and current. In these scheme the most important block is the

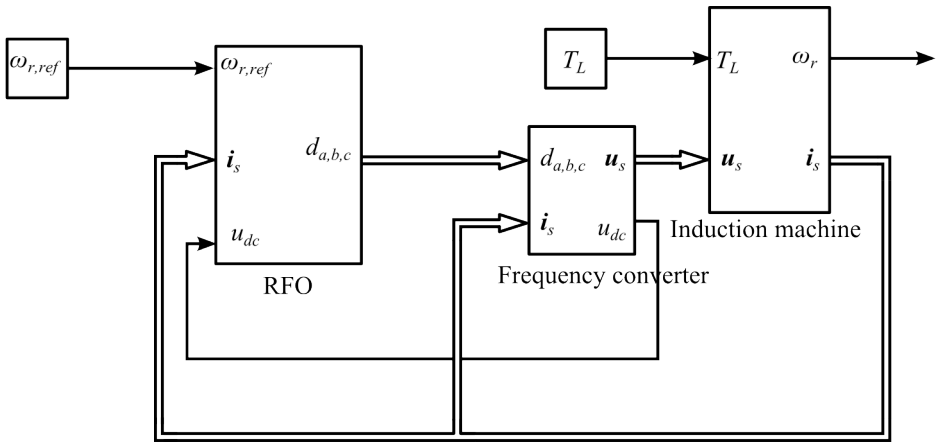

Figure 5.1: Full simulation model of the IM vector control

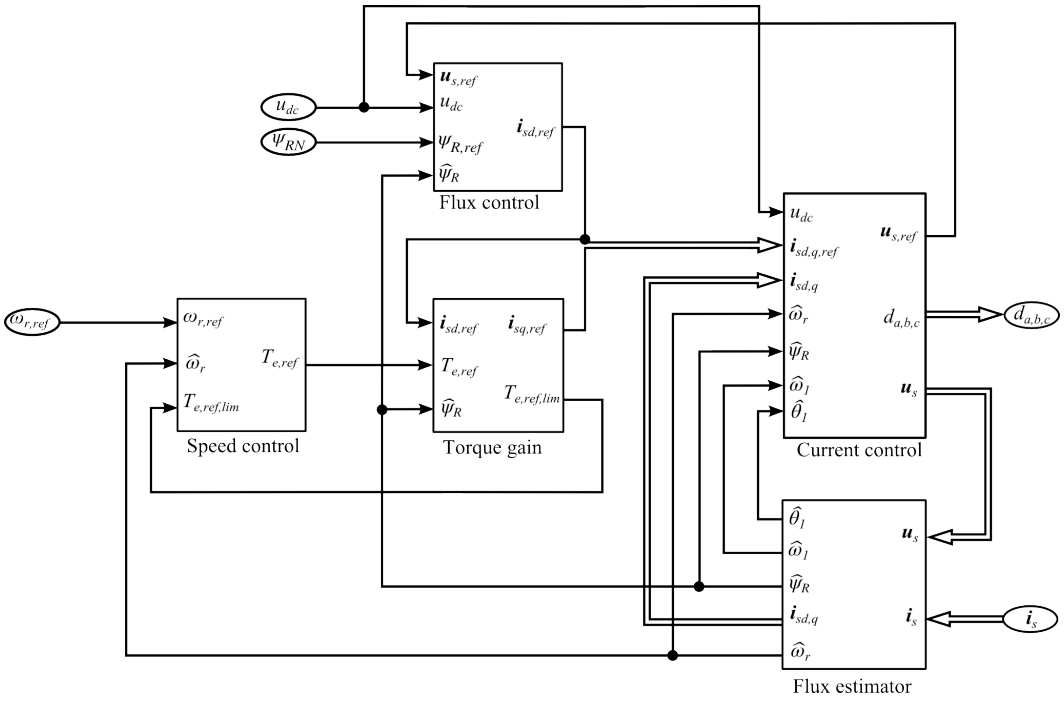

Figure 5.2: RFO block scheme

"Flux estimator". The "Flux estimator" provides all the other blocks with estimated values of the rotor flux, the speed, and the angle of the flux. It also provides the coordinate transformation from stator reference to synchronous coordinates. The "Current control" block receives the estimated values plus the reference for the current which is provided by the "Speed control" and "Flux control" blocks and calculates the duty cycles which are already transformed in stator coordinates and fed to the frequency converter.

The blocks in the "RFO" scheme are programmed using S-function blocks which are written in the C language. The simulated motor is an 2.2 kW induction machine (ABB M2AA 100 LA). The motor's parameters are shown in Tables 5.1-5.3.

Table 5.1: Base values of the induction machine

Base value	Symbol and formula	Value	Unit
Voltage	$u_B = \sqrt{2/3}U_N$	326.60	V
Current	$i_B = \sqrt{2}I_N$	7.07	A
Frequency	$f_B = f_N$	50	Hz
Angular frequency	$\omega_B = 2\pi f_N$	314.16	rad/s
Power	$1.5u_B i_B$	3464	W
Flux	$\psi_B = u_B/\omega_B$	1.04	Wb
Torque	$T_B = p \cdot p_B/\omega_B$	22.05	Nm
Impedance	$Z_B = u_B/i_B$	46.19	Ω
Inductance	$L_B = Z_B/\omega_B$	0.15	H
Capacitance	$C_B = 1/(\omega_B Z_B)$	0.69	μF

Table 5.2: Rated values of the induction machine

Rated value	Symbol and formula	Value	Unit
Power	P_N	2200	W
Voltage	U_N	400	V
Current	I_N	5	A
Frequency	f_N	50	Hz
Rotational speed	n_N	1436	rpm
Angular frequency	$\omega_{1N} = 2\pi f_N$	314.16	rad/s
Pole pairs	p	2	-
Torque	T_N	14.06	Nm
Power factor	$\cos\phi_N$	0.79	-

Table 5.3: The inverse-Γ model circuit parameters in p.u. values

Parameter	Symbol	Value	Unit
Stator resistance	R_s	0.064	p.u.
Rotor resistance	R_R	0.0347	p.u.
Total leakage inductance	L_σ	0.17	p.u.
Magnetizing inductance	L_M	2.1556	p.u.

5.3 Simulation results and observations

5.3.1 Normal operation cases

There have been four simulation scenarios that were taken into account for testing the full order observer designs, which will be referred as Cases 1-4. Case 1 consists of a series of load operations. This scenario starts with the velocity of the machine set at zero. After 1 second there is a stepwise increase in the speed to half of the nominal speed. After reaching the indicated speed, a nominal load is applied then removed in a span of one second. The simulation is ending by reducing the machine speed all the way to zero.

In Case 2 a high speed operation is simulated. The simulation starts at zero speed and continues so for 0.5 seconds, when the speed increases stepwise at the value of 1.5 p.u. There is also a nominal load applied while running at high speed, at the 1.5 seconds mark.

Case 3 is that of a slow speed reversal, which is the most challenging operation for an induction speed. This case was simulated beginning from half the nominal speed (0.5 p.u.) to the same value in negative. The first speed reversal process takes 15 seconds to achieve, after which the reference speed is changed back to the initial speed.

Case 4 consists of two Case 2 sequences one after each other. In the following figures, the performance of the two observer designs mentioned in the previous chapter is simulated.

Original design

In the first four figures, Figures 5.3-5.6, is shown the original design [3]. For the simulation there was a need to set values to the following tuning parameters: γ_i, γ_p, which are the gains for the speed adaptation law used in the observer, and ω_{min} which is a tuning parameter specific to the original design.

The original observer design [3] has been quite difficult to tune, due to lack of flexibility. The smallest changes in the parameters renders the simulation in error. To be more specific one of the variables reaches zero which causes MATLAB to give an error of division by zero. Nevertheless, successful simulations for the four cases described above were achieved by setting two sets of values for the parameters. For Cases 1, 2, and 4 the following values were used:

$$\begin{aligned} \gamma_i &= 0.07, \\ \gamma_p &= \frac{L_\sigma}{r} k_i, \\ \omega_{min} &= 0.04. \end{aligned}$$

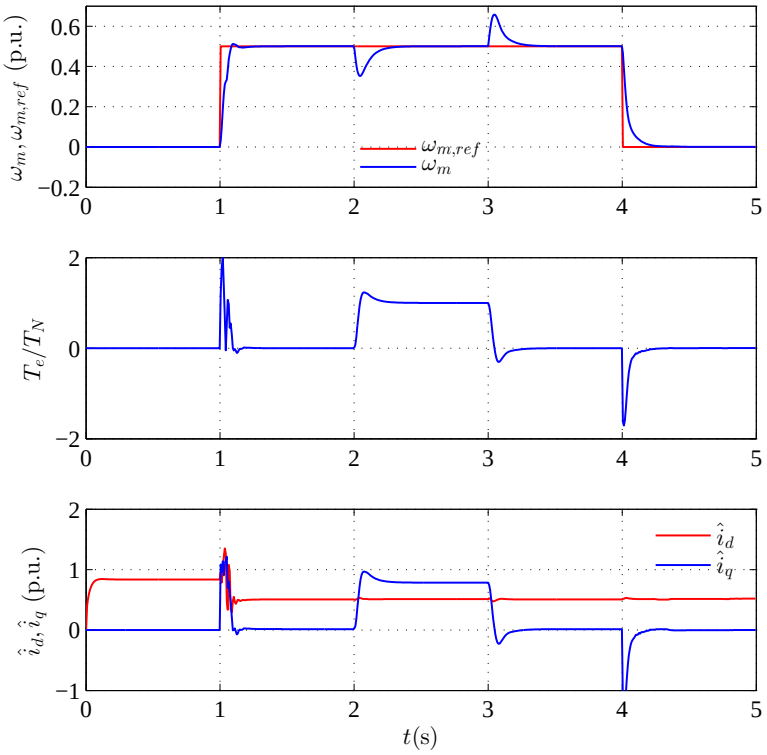

Figure 5.3: Simulation waveforms for Case 1 for the original design proposed in [3]

And for Case 3:

$$\gamma_i = 0.07,$$
$$\gamma_p = \frac{L_\sigma}{r} k_i,$$
$$\omega_{min} = 0.05.$$

Figure 5.3 shows the waveforms in Case 1 for the original design [3], where the ω_m and ω_m, ref represent the mechanical rotor speed and its reference, the T_e/T_N is the electromagnetic torque in p.u., and $\hat{i}_d$, $\hat{i}_q$ are the components of the estimated stator current in synchronous coordinates. The simulation seems to be working normally, with the exception of small disturbances in the currents, i_d and i_q, and torque, when there is an increase from 0 to 0.5 p.u. in speed. Due to those disturbances, a small overshoot can be seen in the speed. This happens because the design parameter l has the value zero for when the speed is zero, causing an erroneous calculation of the rotor flux estimate. Hence the observer gives a higher estimate of the current i_d.

In Figure 5.4, Case 2 is displayed. This simulation has resulted with two big overshoots in speed after which there are another two quite small overshoots in an attempt to adjust the speed to the value of 1.5 p.u. It can be clearly seen that the overshoots are caused by the instability in the currents, i_d and i_q depicted in the third plot in the figure. By applying a load at 1.5 seconds, the machine has a lower

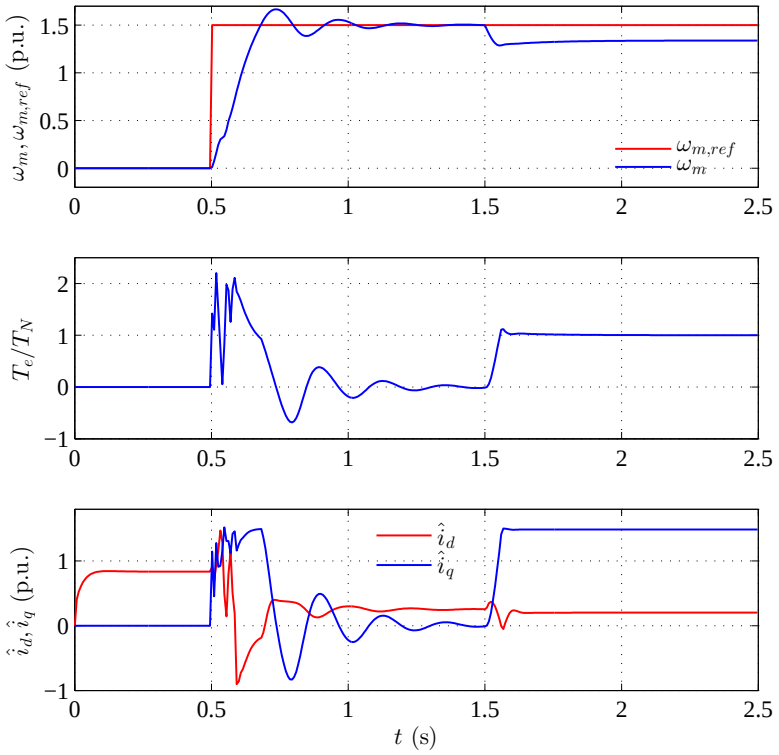

Figure 5.4: Simulation waveforms for Case 2 for the original design proposed in [3]

speed than the reference. This phenomena is caused because the voltage cannot be increased further than nominal, in order for the speed to reach the reference.

Figure 5.5 represents Case 3, where a slow speed reversal is simulated. At a second after the simulation has started a load was applied, which can be identified by the small drop in speed at the beginning of the waveform but the speed has been corrected easily. The machine performs the speed reversal without any problems, hence the estimated values are following the reference quantities properly.

Case 4 is shown in Figure 5.6. This simulation was done to see how the design behaves with repeated sequences. The first sequence goes in same way as in Case 1. But when the second sequence starts, i_d stays constant as it can be seen in the third plot, hence the speed increases smoothly to the speed reference of 0.5 p.u. and there is no overshoot anymore.

Improved design

The following figures show the cases simulated with the improved design, [4]. This design has been very easy to tune. The design parameters do not affect the operation drastically, unlike the original design. Figure 5.7 shows a smooth start, the speed increases steadily. At the same time the i_d starts at a proper value, about 0.5 p.u., when for the original design the i_d has a value of 0.8 p.u., which was too big. Also it is noticed that there is no overshoot when the speed reaches the reference, unlike in the case for the original design where there was an overshoot before the

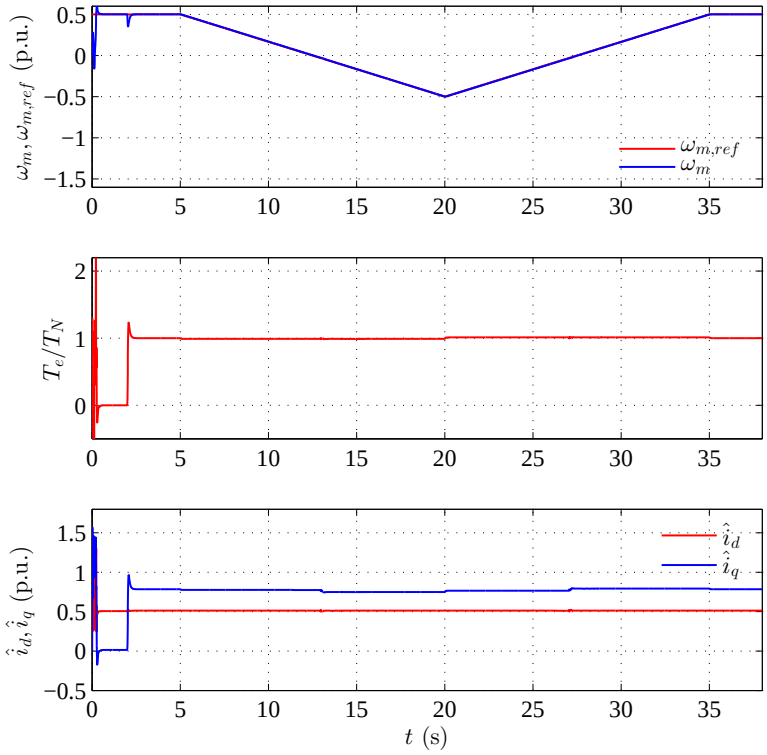

Figure 5.5: Simulation waveforms for Case 3 for the original design proposed in [3]

stabilization of the speed. The speed is constant at 0.5 p.u. in under 250 ms, but the original design takes about 250 ms also until the speed is constant.

The high speed operation (Case 2), shown in Figure 5.8, is carried out without difficulty. There is a huge improvement from the original design, Figure 5.4. It is running smoothly, reaching reference value in little after 250 ms, compared to the original design where the speed does not stabilize in the 1.5 seconds before the load is applied. There are no overshoots present. When the load is applied the speed is constant in about 65 ms after, opposed to the original design, which it takes more than 250 seconds to remain at constant value.

Finally Case 3 is illustrated in Figure 5.9. The speed reversal runs smoothly, no visible disturbances in the speed except for when the load is used, which is a normal phenomena.

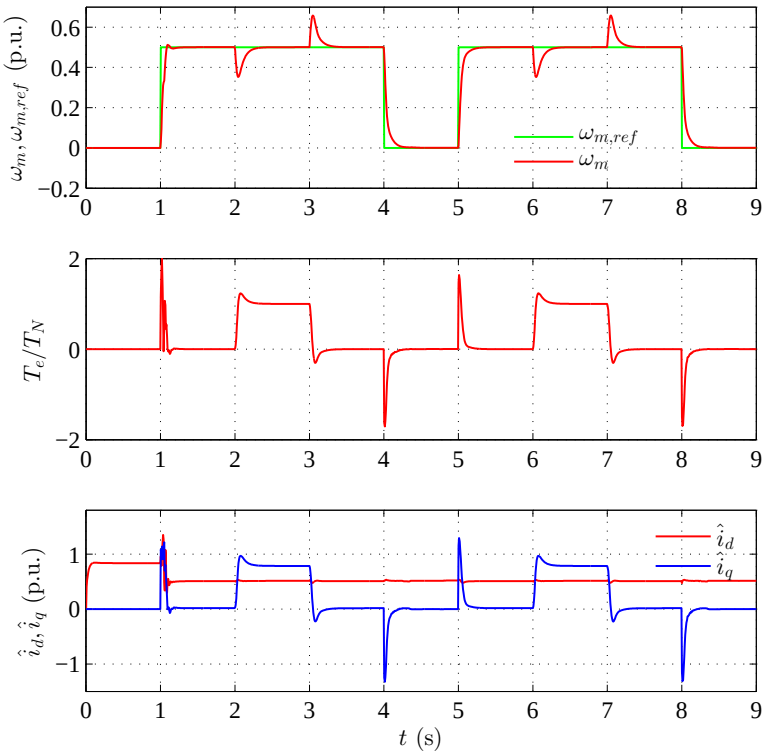

Figure 5.6: Simulation waveforms for Case 4 for the original design proposed in [3]

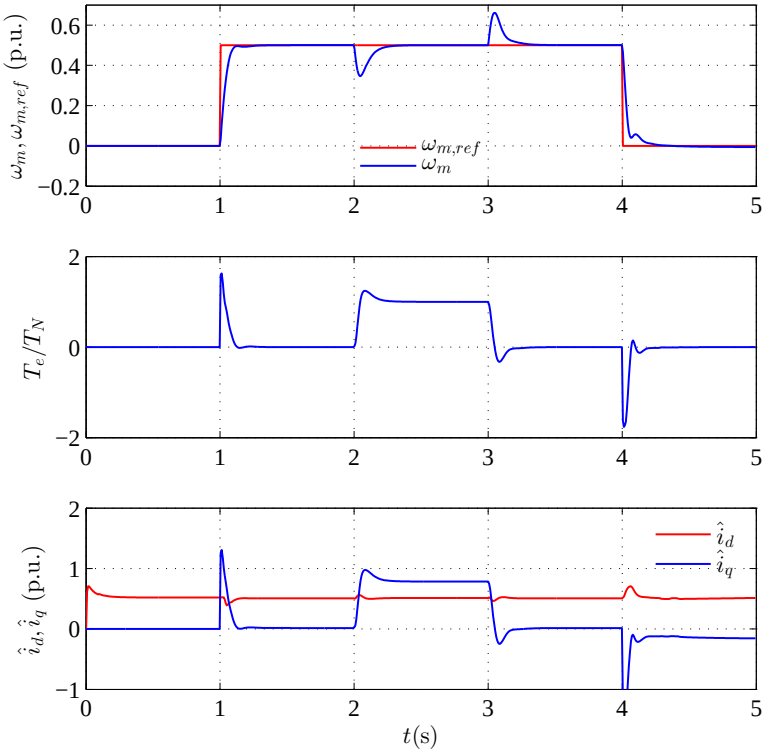

Figure 5.7: Simulation waveforms for Case 1 for the improved design proposed in [4]

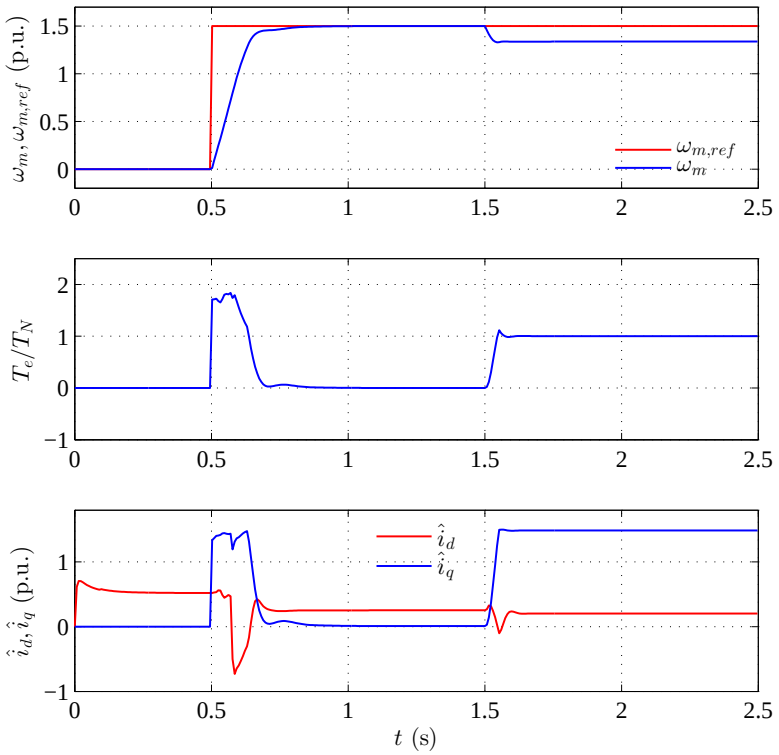

Figure 5.8: Simulation waveforms for Case 2 for the improved design proposed in [4]

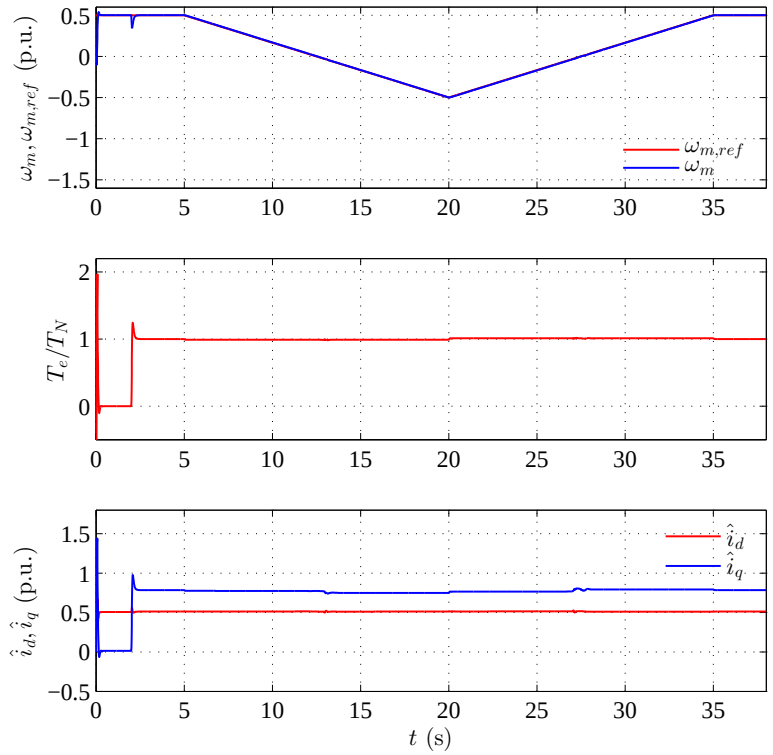

Figure 5.9: Case 3 simulation waveforms for the improved design proposed in [4]

5.3.2 Stator resistance test

A series of simulations have been done in order to discover how the full-order observer designs are behaving facing different percentage of error in stator resistance.

These tests are beneficial because in practice, the stator resistance of the machine changes according to temperature. The temperature can change considerably while the machine is running. Hence the full order observer needs to be able to withstand changes in resistance.

The stator resistance error was applied to the estimated stator resistance parameter, the one used in the observer's algorithm. This means the simulation is a situation where the observer uses a stator resistance different than the actual stator resistance of the machine.

Original design

The trials for the original design were not satisfactory. A trial for a very small error, $\hat{R}_s = 1.0001 R_s$, has been shown in Figure 5.10. In Cases 2 and 3, the waveforms plotted for the original design are the same as without error, $\hat{R}_s = R_s$, see Figures 5.4 and 5.5. But for Case 1 the design does not cope with the minor error and is not working at all. It can be seen that the system is highly unstable having huge oscillations in speed and torque, Figure 5.10a.

At an error of $\hat{R}_s = 1.0005 R_s$ the simulation crashes completely. For Cases 1 and 3 the simulation gets interrupted at 0.06025 second and 0.0355 second, respectively, which means that either flux or speed have reached 0 or infinite which causes MATLAB to generate an error of positive or negative infinity. In Case 2 the speed is totally unresponsive remaining 0 for the whole time, except some oscillations when speed is increased and when the load is put.

This shows that the original design has a high sensitivity for the stator resistance. Further tuning will be necessary for establishing successful simulations when the stator resistance changes. This could be done, but it cannot be put into practice. Tuning cannot be done in matter of seconds while the machine is working. The only viable solution would be to eliminate the dependency on the stator resistance.

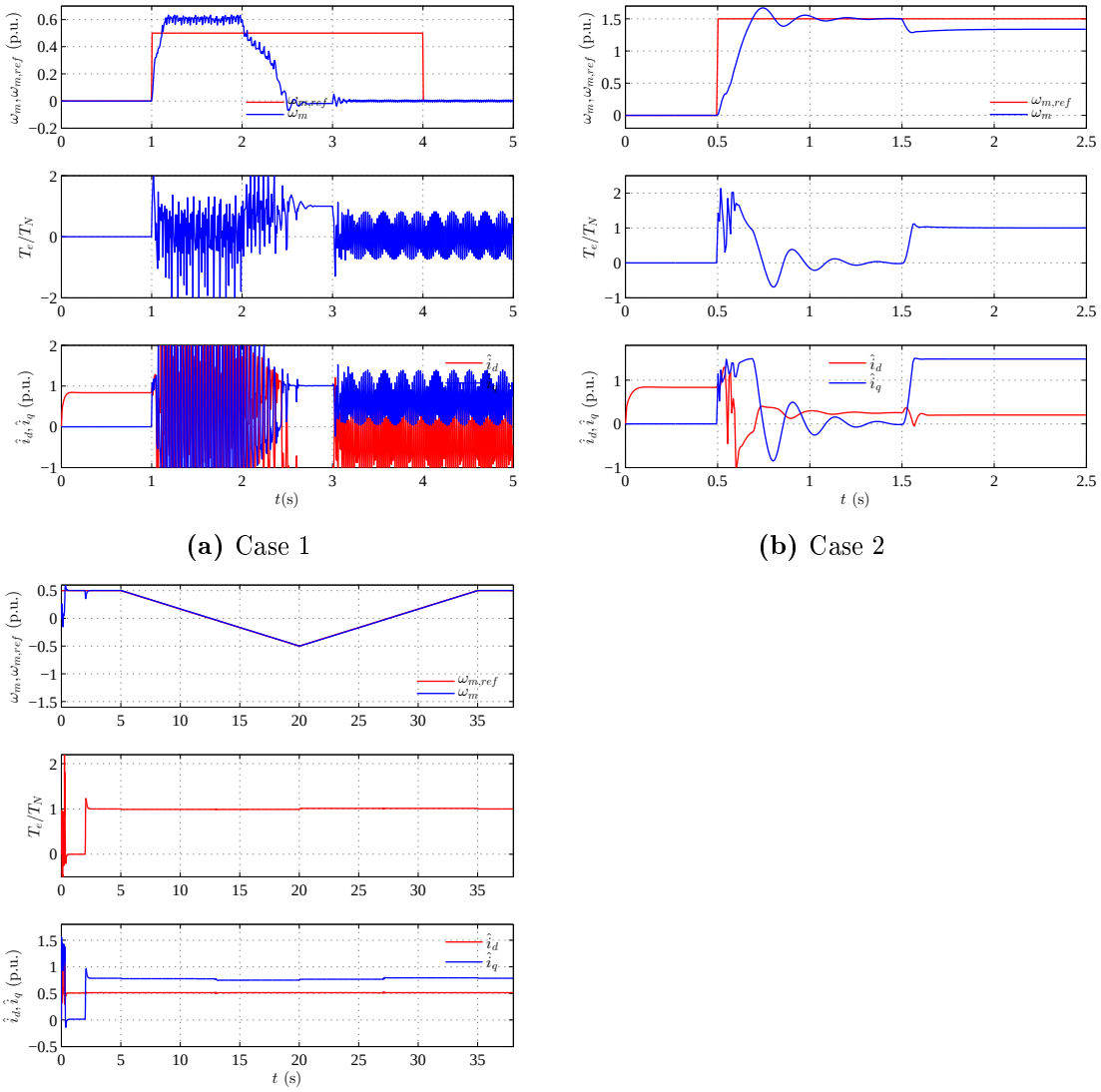

(a) Case 1

(b) Case 2

(c) Case 3

Figure 5.10: Simulation waveforms of the original design, [3], for $\hat{R}_s = 1.0001R_s$ error

Improved design

The trials for the improved design have yielded better results. The design was tested for stator resistance errors from $\hat{R}_s = R_s \pm 0.01R_s$ to $\hat{R}_s = R_s \pm 0.30R_s$.

On overall the design has functioned very well for Cases 1 and 2, having no visible disturbance in the speed and torque waveforms. Hence the improved observer design handles the errors for stator resistance in applications that include normal speeds and high speed operation. For these cases, [4] has made a great progress, making the design stable and working for estimation errors in stator resistance, while the original design is not able to run the simulations at all.

On the other hand Case 3 is a challenge for this design as well. In Case 3 the machine has to do a speed reversal, which means the machine has to cross two times

a region where $\omega_1 = 0$, these regions are very problematic for sensorless drives.

The design is not affected by the error $\hat{R}_s = R_s \pm 0.01R_s$ in the stator resistance. Normal operation of the improved design is witnessed for an underestimated error where $\hat{R}_s = 0.96R_s$ and until the overestimated error $\hat{R}_s = 1.02R_s$, like in Figures 5.7-5.9.

Figure 5.11a represents an example of the waveforms that the improved design has for errors between $\hat{R}_s = 1.02R_s$ and $\hat{R}_s = 1.06R_s$. The speed passes successfully through $\omega_1 = 0$ the first time, but the second time the system crashes, the speed remaining zero.

When the error is increased further than $\hat{R}_s = 1.06R_s$ the waveforms follow the ones in Figure 5.11b, which surprisingly has only a small disturbance in the $\omega_1 = 0$ zone both times. As the error is further increased the disturbance becomes bigger and bigger until the system becomes unstable which was at the overestimation of $\hat{R}_s = 1.30R_s$.

Although the system runs smoothly until an error of $\hat{R}_s = 0.96R_s$ at $\hat{R}_s = 0.95R_s$ the system crashes, as can be seen in Figure 5.12a the speed is decreasing and does not manage to come back to the reference at all. For an error of $\hat{R}_s = 0.85R_s$ the system manages to come back to the reference having a spike where the speed decreases to the $\omega_1 = 0$ point, but it crashes at the second crossing.

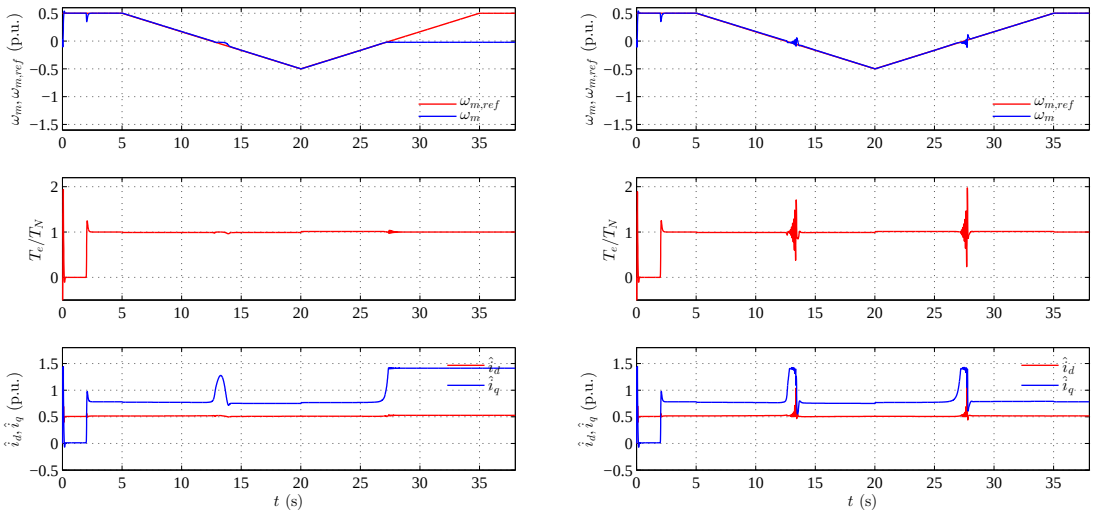

(a) $\hat{R}_s = 1.05R_s$ **(b)** $\hat{R}_s = 1.10R_s$

Figure 5.11: Simulation Case 3 waveforms of the improved design, [4], for stator resistance overestimation

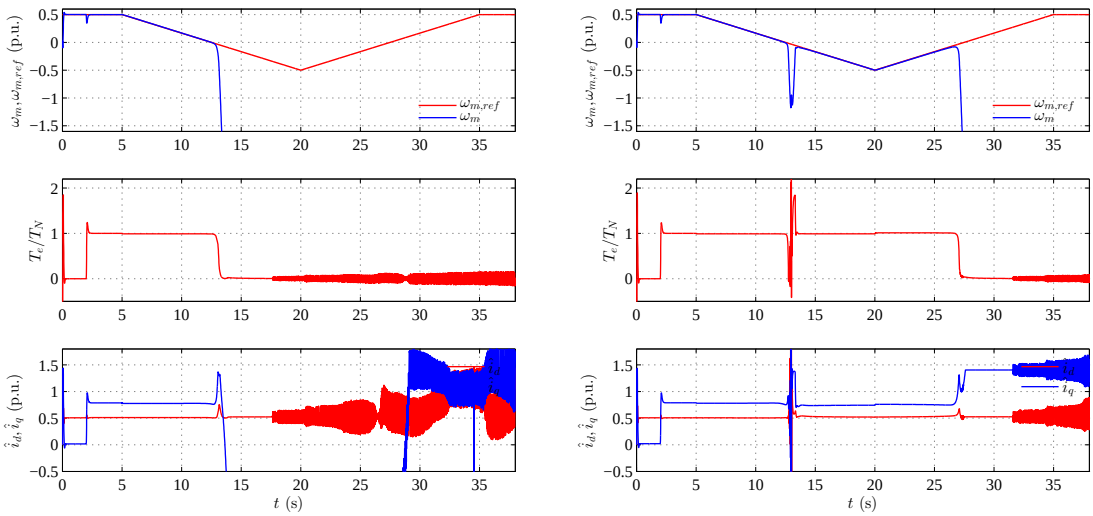

(a) $\hat{R}_s = 0.95R_s$ **(b)** $\hat{R}_s = 0.85R_s$

Figure 5.12: Simulation Case 3 waveforms of the improved design, [4], for stator resistance underestimation

6 Discussion and conclusion

In this thesis the main topic is the full-order observer. Two new and promising designs have been chosen, [3] and [4], in order to analyse them.

The full-order observer designs were simulated for a 2.2 kW induction motor in MATLAB/Simulink. The simulation cases, that were considered for testing the FOO designs, represent operations that the induction machine can do in certain applications. The simulations include load operations at normal speed, high speed operation with and without load, and speed reversal.

While trying to implement the original design [3] into the simulation model, the design has proved to be very hard to tune. Slight changes in the tuning parameters would render the simulation not working due to the flux or speed having either zero or infinite value. The tuning parameters γ_i, γ_p, the gains for the speed adaptation law, and ω_{min} which is specific to the original design, were found by trial and error. Two sets of parameters were found to work for the cases simulated. With the chosen parameters the full-order observer runs nicely for normal speed operations with some load manoeuvres and for speed reversals, but for high-speeds the simulation runs with oscillations while the design is trying to stabilize the speed to the reference. After the stator resistance error test was conducted, it has been concluded that the design does not present tolerance to changes in stator resistance.

The design in [4] is a great improvement to the original design [3] as it was able to successfully overcome the latter's shortcomings. While the simulations were conducted it has been noticed that the design is very flexible concerning the tuning parameters mentioned above, which makes the tuning of the full-order observer an easy task. The design has performed very well in all cases simulated, a visible improvement is noticed in the high-speed operation. After the stator resistance error trials, it shows that the changes have improved the tolerance of the design for changes in stator resistance.

The most known problem of sensorless IM drives is the low-speed operation, mainly when the motor operates in regenerative mode. This problem has been remedied by [4] to a certain point. The design can withstand an underestimated error of up to -4% and an overestimated error of up to $+2\%$ in the stator resistance without affecting the stability of the system. Increasing further the error the instability at the low speed region can be seen. Further research would be needed if the stability is wanted with larger estimation errors.

The computer simulations for this thesis have not included a stator resistance adaptation scheme. By implementing an adaptation scheme for stator resistance, it can improve the results of the simulations for both designs.

Stability tools have not been used to determine the stability sources in this thesis. Future work can be done using some stability tools such like the linearisation model proposed in [15] in order to analyse more thoroughly the designs chosen in this thesis.

7 References

[1] L. Harnefors, M. Hinkkanen, "Stabilization of sensorless induction motor drives: a survey," in *IEEE Workshop on Electrical Machines Design, Control and Diagnosis*, Paris, France, Mar. 2013.

[2] H. Kubota, K. Matsuse and T. Nakano, "DSP-based speed adaptive flux observer of induction motor," *IEEE Transactions on Industry Applications*, vol. 29, no. 2, pp 344-348, Mar./Apr. 1993.

[3] S. Sangwongwanich, S. Suwankawin, S. Po-ngam and S. Koonlaboon, "A unified speed estimation design framework for sensorless AC motor drives based on positive-real property" in *Proc. PCC-Nagoya'07*, Nagoya, Japan, pp 1111-1118, Apr. 2007.

[4] Q. Zengcai, M. Hinkkanen, L. Harnefors, "Gain scheduling of a Full-Order Observer for Sensoreless Induction Motor Drives,", in *Sensorless Control for Electrical Drives and Predictive Control of Electrical Drives and Power Electronics (SLED/PRECEDE)*, Munich, Germany, Oct. 2013.

[5] G.R. Slemon, "Modelling of induction machines for electric drives," *IEEE Transactions on Industry Applications*, vol. 25, no. 6, pp 1126-1131, Nov./Dec. 2004.

[6] J. Holtz, "Sensorless Control of induction motor drives," *Proceedings of the IEEE*, vol. 90, no. 8, pp 1359-1394, Aug. 2002.

[7] R. de Doncker, D.W.J. Pulle, A. Veltman "Advanced electrical drives - analysis, modelling, control," Springer Netherlands, 2011.

[8] L. Harnefors, "Control of variable-speed drives," *Compendium*, Mälardalen University, Västerås, Sweden, 2003.

[9] M. Hinkkanen, "Flux estimators for speed-sensorless induction motor drives," *Ph.D. dissertation*, Helsinki University of Technology, Espoo, Finland, 2004.

[10] M. Hinkkanen and J. Luomi, "Parameter sensitivity of full-order flux observers for induction motors," *IEEE Transactions on Industry Applications*, vol. 39, no. 4, pp 1127-1135, Jul./Aug. 2003.

[11] G.C. Verghese and S.R. Sanders "Observers for flux estimation in induction machines," *IEEE Transactions on Industry Applications*, vol. 35, no. 1, pp 85-94, Feb. 1988.

[12] L. Harnefors, "Design and analysis of general rotor-flux-oriented vector control systems," *IEEE Transactions on Industrial Electronics*, vol. 48, no. 2, pp 383-390, Apr. 2001.

[13] C. Schauder, "Adaptive speed identification for vector control of induction motors without rotational transducers," *IEEE Transactions on Industry Applications*, vol. 28, no. 5, pp 1054-1061, Sept./Oct. 1992.

[14] L. Harnefors, M. Hinkkanen, "Complete stability of reduced-order and full-order observers for sensorless IM drives," in *IEEE Transactions on Industrial Electronics*, vol. 55, no. 3, pp 1319-1329, Mar. 2008.

[15] M. Hinkkanen, "Analysis and design of full-order flux observers for sensorless induction motors," *IEEE Transactions on Industrial Electronics*, vol. 51, no. 5, pp 1033-1040, Oct. 2004.

[16] F. Alonge, F. D'Ippolito, G. Giardina, and T. Scaffidi "Design and low-cost implementation of an optimally robust reduced-order rotor flux observer for induction motor control," *IEEE Transactions on Industrial Electronics*, vol. 54, no. 6, pp 3205-3216, Dec. 2007.

[17] M. Hinkkanen, L. Harnefors, and J. Luomi "Reduced-order flux observers with stator-resistance adaptation for speed-sensorless induction motor drives," in *Energy Conversion Congress and Exposition (ECCE 2009)*, San Jose, CA, pp 155-1623, Sept. 2009.

[18] G. Yang and T.-H. Chin, "Adaptive-speed identification scheme for a vector-controlled speed sensorless inverter-induction motor drive," *IEEE Transactions on Industry Applications*, vol. 29, no. 4, pp 820-825, Jul./Aug. 1993.

[19] M. Hinkkanen and J. Luomi, "Digital implementation of full-order flux observer for induction motors," in *Proc. EPE-PEMC'02*, Cavtat and Dubrovnik, Croatia, CD-ROM.

[20] M. Hinkkanen and J. Luomi, "Stabilization of regenerating-mode operation in sensorless induction motor drives by full-order flux observer design," *IEEE Transactions on Industrial Electronics*, vol. 51, no. 6, pp 1318-1328, Dec. 2004.

[21] L. Harnefors and H.-P. Nee, "Full-order observers for flux and parameter estimation of induction motors," in *Proc. EPE'97*, vol. 3,Trondheim, Norway, pp 375-381, Sept. 1997.

[22] L. Harnefors, "Globally stable speed-adaptive observers for sensorless induction motor drives," *IEEE Transactions on Industrial Electronics*, vol. 54, no. 2, pp 1243-1245, Apr. 2007.

[23] M. Hinkkanen and J. Luomi, "Novel full-order flux observer structure for speed sensorless induction motors," in *The 27th Annual Conference of the IEEE Industrial Electronics Society (IECON'01)*, vol. 2, Denver, CO, pp 1333-1338, Nov/Dec. 2001.